

Characteristics of Ethylene–Methyl Methacrylate Copolymer and Ultrahigh Molecular Weight Polyethylene Composite Filled with Multiwall Carbon Nanotubes Prepared by Gelation/Crystallization from Solutions

Qingyun Chen, Yuezhen Bin, and Masaru Matsuo*

Department of Textile and Apparel Science, Faculty of Human Life and Environment, Nara Women's University, Nara 630-8263, Japan

Received January 31, 2006; Revised Manuscript Received July 12, 2006

ABSTRACT: Ultrahigh molecular weight polyethylene (UHMWPE) and ethylene–methyl methacrylate copolymer (EMMA) composites containing multiwall carbon nanotubes (MWNTs) were prepared by the gelation/crystallization method. The conductivity and Young's modulus were obtained as a function of EMMA content. When 5 wt % MWNT was admixed into neat EMMA known as an insulator, conductivity of the composite reached ca. 0.05 S/cm, which was much higher than the conductivity of UHMWPE with 5 wt % MWNT. The UHMWPE/EMMA–MWNT composite containing 14 wt % EMMA and 5 wt % MWNT could be stretched up to 50 times. The conductivity and Young's modulus reached 3.84×10^{-3} S/cm and 37 GPa, respectively, which denoted a successful result for preparing a conductive material with high modulus. The electrical conductivity of the composite increased with increasing draw ratio, indicating that the band gap became narrower by elongation. Furthermore, the conductivity increased with elevating temperature, but it tended to decrease beyond the melting point of the composites. Such a temperature dependence of the conductivity is perfectly different from the characteristics of polymer–carbon fiber and polymer–carbon black particles reported already. Such interesting phenomena were mainly analyzed by using X-ray and scanning electron microscopy in terms of morphological aspects.

1. Introduction

Multiwall carbon nanotubes (MWNTs) have been expected as attractive fillers for increasing the electrical conductivity of polymers at relatively low MWNT content.^{1–5} This efficient behavior is attributed to their excellent theoretical electrical properties beyond copper and their mechanical properties beyond diamond.^{6–8} Polymer–MWNT composite provided the percolation concentration between 1 and 5 vol %^{9–11} because of the formation of continuous networks ensuring conductive paths, which is characteristic properties of MWNTs with high aspect ratio and flexibility.¹² Actually, the critical values are much lower than the filler concentration needed for percolation in systems with carbon black or metallic fillers.^{13–16} In addition to improvement of conductivity, MWNTs also have played an important role to improve the modulus and strength of the composites as reinforced fillers.^{17–21}

It is well-known that polymer–MWNT interactions include (a) multicontact of polymer chains on the surface of MWNTs (physicosorption), (b) reactions of MWNTs with polymers (chemisorption), and (c) mechanical chain entanglements and covalent carbon–carbon cross-link in the polymer matrix.^{22,23} These interactions obviously cause the influence on electrical conductivity and mechanical properties of the composite. The present MWNTs are composed of graphene sheets with defects fewer than the previous MWNTs as their own properties¹⁷ and then induce hard dispersion of such MWNTs into the matrix of ultrahigh molecular weight polyethylene (UHMWPE). The MWNTs were dispersed uniformly within the mixed solution of UHMWPE and ethylene–methyl methacrylate copolymer (EMMA) which were prepared in accordance with a previous successful method.²⁴ In EMMA chains, there are the polar side

groups (–C=O) in the alkyl main chains. The dispersion of MWNTs in the UHMWPE/EMMA matrix could be improved drastically. In accordance with the previous method,²⁴ the present composite materials containing MWNTs were prepared by gelation/crystallization from solutions because the gelation/crystallization method has been well-known as a powerful technique to prepare UHMWPE–MWNT composite with the greatest drawability.¹⁷ Also, the method was more effective than the kneading method, when carbon fibers or particles were dispersed uniformly into polymer matrix with high melting viscosity. Apart from the present method, a new method was reported recently by Zhang et al.²⁵ for uniform dispersion of single wall carbon nanotubes (SWNTs) and UHMWPE. According to their report, the dispersion was carried out by spraying an aqueous solution of SWNTs onto a fine UHMWPE powder directly obtained from synthesis, since the SWNTs were absorbed on the surface of the powder. A composite film was prepared from the solution of the powder dissolved in xylene, which was based on their experimental result that the high viscosity of UHMWPE in solution prevented the coaguration of the absorbed SWNTs.

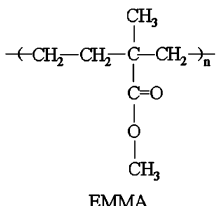
This paper deals with the successful preparation of composites with high modulus and high electrical conductivity by admixing small amount of MWNT content into UHMWPE/EMMA matrix. The detailed analysis of the successful origin is carried out in terms of morphological aspects by using scanning electron microscopy (SEM), X-ray, and differential scanning calorimetry (DSC).

2. Experiment

The polymer materials used in the present work were UHMWPE produced by Mistui Chemical Co. Ltd. and EMMA furnished by Sumitomo Chemical Co. Ltd. Some properties of these polymers are listed in Table 1. The detailed characteristics were described elsewhere.^{26,27}

* To whom correspondence should be addressed: Tel/Fax (81)-742203462; e-mail m-matsuo@cc.nara-wu.ac.jp.

Table 1. Some Properties of the Used Polymers

Specimen	MMA (mol %)	mp (°C)	\bar{M}_n^a	\bar{M}_v^b	 EMMA
EMMA	14.6	64	3.1×10^4		
UHMWPE		142		6×10^6	

^a \bar{M}_n = average number molecular weight. ^b \bar{M}_v = average viscosity molecular weight.

Figure 1a,b shows photo images of the MWNTs observed by SEM (JEOL 6700). Image (b) is the enlargement of image (a), which shows uniform diameter distribution of the MWNTs prepared by vapor ablating technique. Figure 1c shows a Raman spectrum at excitation laser wavelength of 488 nm. The image (a) indicates the MWNTs possess many irregularly shaped particles, which were confirmed to be carbon elements by energy dispersive spectroscopy (EDS). They could not be removed by concentrated $\text{H}_2\text{SO}_4/\text{HNO}_3$ (3/1) treatment at elevated temperature. By these treatments, the MWNTs were slightly damaged. In fact, some disrupted MWNTs were cut into very short fibers, which were observed at large magnification of SEM observation. Then the original MWNTs were used in this study. The Raman spectrum shows a sharp large peak at about 1562 cm^{-1} termed as G-band,^{28,29} which is associated with Raman-allowed phonon mode E_{2g} and a duller small peak at about 1334 cm^{-1} termed as D-band, which is associated with the disordered-induced phonon mode due to the infinite size of crystals and defects. In this case, the irregularly shaped particles take a great role in effect of D-band. The present MWNTs with a diameter (D) of 10–50 nm, a length (L) of 10–20 μm , and the aspect ratio (L/D) of $(1-2) \times 10^3$ could be obtained. The MWNTs tend to form bundles of nanotubes like single-wall carbon nanotubes (SWNTs) reported already. The two peaks indicate that the present MWNTs used in this experiment have a higher degree of graphitization than the previous MWNTs (Hyperion Graphite Fibers) used to prepare ultradrawn polyethylene–MWNTs composites with high modulus and high electric conductivity.¹⁷ From preliminary experiments, as discussed before, the uniform dispersion of the present MWNTs with high order curved graphene sheets into the UHMWPE matrix was confirmed to be slightly difficult, and then small amounts of EMMA were admixed into the UHMWPE. The composite of the UHMWPE against the EMMA was termed as the UHMWPE/EMMA.

In preparing the homogeneous UHMWPE/EMMA–MWNT composites, the concentration of UHMWPE against decalin was fixed to be 1 g/100 mL decalin. Through trial and errors, it was found that the concentration was the optimum condition to ensure uniform dispersion of the MWNTs in the present UHMWPE and EMMA mixed solution. First of all, the MWNTs in decalin were treated more than 24 h using ultrasonic by batch operation with every 20 min interval (treated for 15 min and stopped for 5 min) at room temperature. After then, the UHMWPE and the EMMA were added into the decalin solvent containing the MWNTs, and the mixture was stirred for 30 min at room temperature. The mixture was heated to 150 °C with a mild heating rate of 2–3 °C/min and maintained by stirring for 40 min at 150 °C. The hot homogenized solution was quenched by pouring it into an aluminum tray at room temperature, thus generating a gel. The decalin was allowed to evaporate from the gel under ambient condition. The nearly dry gels were vacuum-dried for 24 h to remove residual trace of decalin. As a preliminary experiment, the effects of residual trace of decalin on chain mobility of the composites was checked by thermogravimetry (TG) for UHMWPE/EMMA blend films as well as UHMWPE/EMMA–MWNT composites with different UHMWPE/EMMA composition, in which the content of MWNTs was fixed at 5% MWNTs. The measurements were done by using TG/DTA 6300 (SII EXSTAR 6000 of Seiko Instrument) at a heating rate of 10

°C/min in an N_2 atmosphere. For all the specimens, it was confirmed that the weight loss does not occur up to 200 °C. Judging from the boiling point (185–193 °C) of decalin, it was concluded that any residual trace of decalin within the specimens could not be detected by TG measurements. FTIR also could not detect the residual trace of decalin. As the further analysis, differential scanning calorimetry (DSC) provided the same melting point for the UHMWPE/EMMA (6/1) films that were vacuum-dried and kept for different periods in the range from 1 to 7 days, indicating that the chain mobility of UHMWPE and EMMA is not affected by the extremely very small residual trace of decalin which cannot be detected by TGA, DSC, and FTIR.

The dried blend film was cut into strips of length 30 mm and width 10 mm. The strip was clamped in a manual stretching device and stretched in a hot oven at 135 °C in an N_2 atmosphere.

Electrical conductivity at room temperature and electrical conductivity against temperature from 30 to 150 °C at the heating rate of 5 °C/min were measured by high resistance measuring device (HR-100, Iwamoto Co. Ltd.). The digital multimeter was used (Advantest R6441A digital multimeter) when the resistance was lower than $10^7 \Omega \cdot \text{cm}$. When the resistance exceeded beyond $10^7 \Omega \cdot \text{cm}$, the measurements were done by using a high-resistance meter (HP 4339B). All of these measurements were carried out in the plane of the film surface. To prepare the test specimens, the composite film was cut into strips of length 25 mm and the width 15 mm. Before measurements, the specimen was polished to level off the both sides smoothly, since contact resistance depends on the sample surface quality. The results were presented as a logarithm of electrical conductivity ($\log(\text{S/cm})$).

Thermal property of the blend film was estimated by DSC (DSC 6200, SII Exstar 6000) from 20 to 180 °C in an N_2 atmosphere. The scanning speed was 5 °C/min.

X-ray measurements were carried out by a 12 kW rotating-anode X-ray generator (Rigaku RAD-ra) with the monochromatic $\text{Cu K}\alpha$ radiation at elevated temperature.^{30,31} The X-ray beam by $\text{Cu K}\alpha$ radiation at 150 mA and 40 kV was monochromatized with a curved graphite monochromator. The complex dynamic tensile modulus was measured at 10 Hz over the temperature range from –150 to 150 °C by using a viscoelastic spectrometer (VES-F) obtained from Iwamoto Machine Co. Ltd. The length of the specimen between the jaws was 40 mm, and the width was about 1.5 mm. The detailed methods were described already elsewhere.³²

3. Results and Discussion

Figure 2 shows the electrical conductivity of EMMA (0/1), UHMWPE (1/0), and the 6/1 composite as a function of the content of MWNTs measured at room temperature. The measurements were carried out to investigate EMMA effect on electrical conductivity. The electrical conductivity increases with increasing the content of the MWNT and tends to level off, indicating the formation of sufficient conductive paths. The conductivity for the EMMA matrix at the platform was the highest among the three specimens, and it tended to level off at ca. 3% MWNT content. In contrast, the value for UHMWPE at the platform was the lowest and the content to reach was ca.

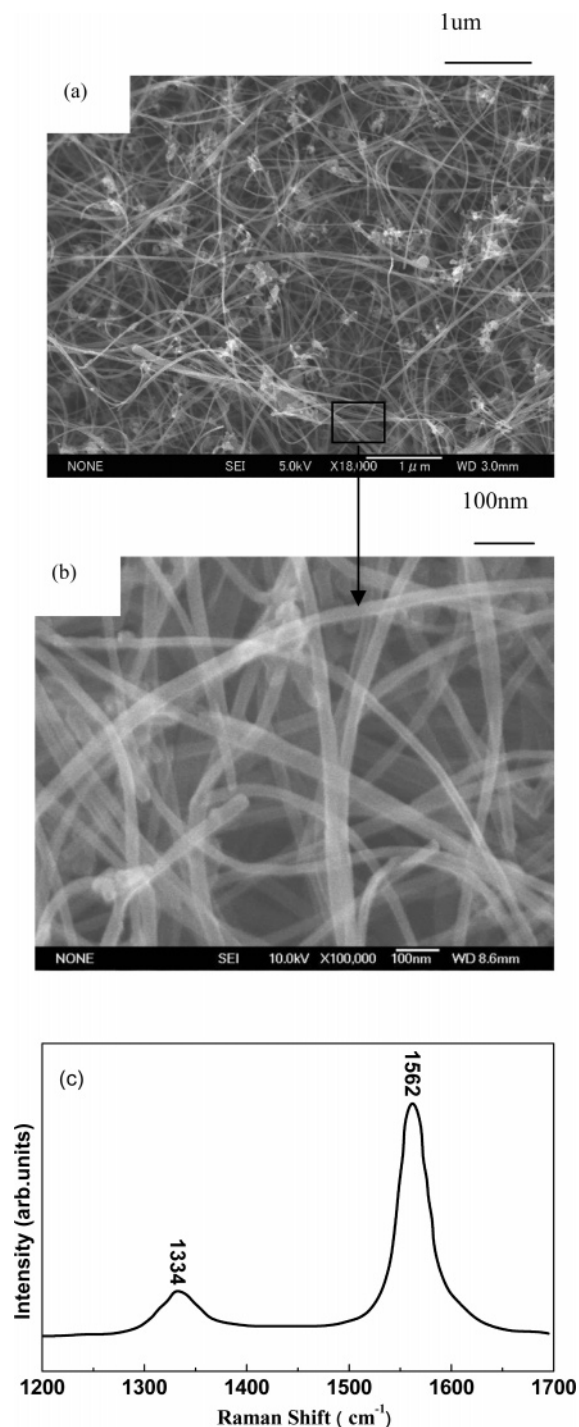


Figure 1. Properties of MWNTs: (a) and (b) are SEM images; (c) is the Raman spectrum.

13% MWNT content. The corresponding platform value for the 6/1 blend was 5% MWNT content. On the basis of the saturation conductivities against MWNT content for the EMMA and the 6/1 composites, the content of the MWNTs in the following experiments was fixed to be 5%.

Parts a and b of Figure 3 show SEM images of the EMMA–MWNT composite, MWNT content being 5%, on the surface area and the cross section area, respectively. It is seen that the dispersed MWNTs in the EMMA matrix form network structures, indicating that 5% MWNT is sufficiently enough to form electric paths. The average diameter of MWNTs in the EMMA matrix is almost the same as that of the original MWNT diameter (see Figure 1). The MWNTs were well-dispersed

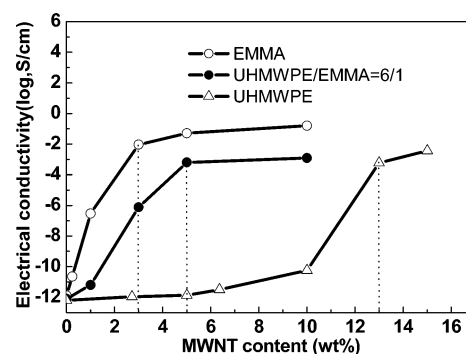


Figure 2. Electrical conductivity of composites as a function of the content of MWNTs (note: MWNTs in UHMWPE is different from those in EMMA and UHMWPE/EMMA).

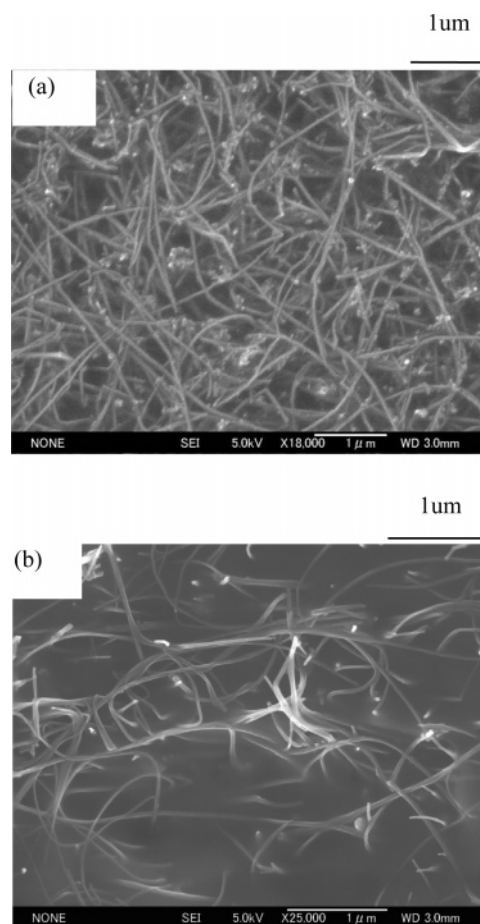


Figure 3. SEM images of EMMA–MWNT composites with 5% MWNTs: (a) surface image; (b) cross-section image.

uniformly in the EMMA solution at 135 °C before generating a gel by quenching. Certainly, it is natural that the surface of each dispersed MWNT was covered by the EMMA layer when the composite was prepared by gelation/crystallization from solution. However, the EMMA layers are too thin to estimate the average thickness from the difference between the average diameter of the dispersed MWNTs in the EMMA matrix in Figure 3a and that of the original MWNTs in Figure 1a.

Parts a and b of Figure 4 show SEM images of the UHMWPE/EMMA–MWNT composite observed on the film surface and cross-section areas, respectively. Interestingly, the MWNTs on the film surface (see photo (a)) are covered by the UHMWPE/EMMA, and their diameters become much thicker than the original diameters (see Figure 1). In contrast, as shown in photo (b), the average diameter of the MWNTs on the cross

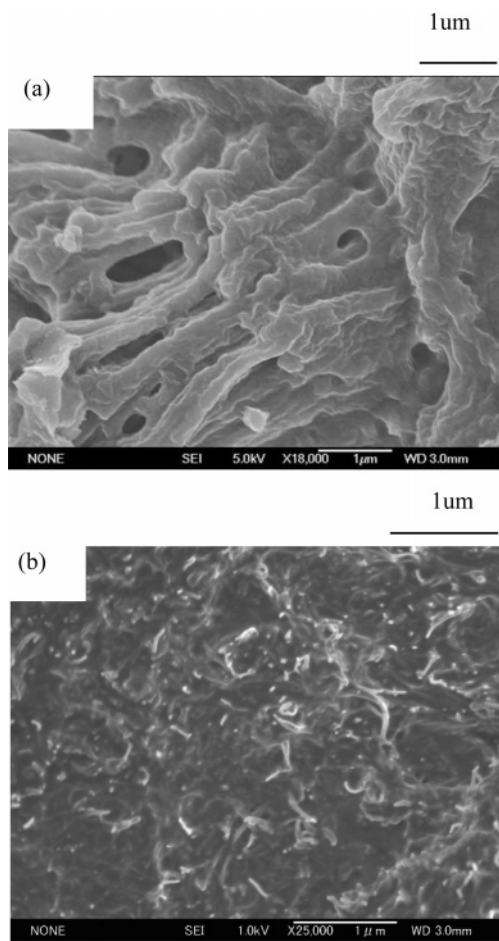


Figure 4. SEM images of UHMWPE/EMMA-MWNT composites with 5% MWNTs: (a) surface image; (b) cross-section image.

section is slightly thicker than that of the original MWNT diameter (see Figure 1a), indicating existence of very small amount of the UHMWPE/EMMA as covering layer. Furthermore, in comparison with Figure 3a, it is reasonable to consider that all the MWNTs were covered by the UHMWPE/EMMA layers which were much thicker than the EMMA layers. Hence, the electron transfer between adjacent MWNTs covered by the UHMWPE/EMMA layer is less active in comparison with the electron transfer between adjacent MWNTs in the EMMA matrix, and then the platform value of conductivity for the UHMWPE/EMMA matrix becomes lower than that for the EMMA matrix, as shown in Figure 2a. Incidentally, on the surface and a cross section, it was confirmed that the SEM images of the UHMWPE composite containing 5% MWNT show slightly thicker in comparison with the layers of the UHMWPE/EMMA (6/1) with the same MWNT content in Figure 4, although the SEM image is not shown in this paper.

To study the significant increase in conductivity by admixing the EMMA into the UHMWPE, the effect of EMMA content on the conductivity of the composite was investigated in the case of 5% MWNT content. They are listed in Table 2, in which each listed data is the average value of the several measurements. The measurements were continued until the reproducibility within the experimental error was beyond 93%. The electrical

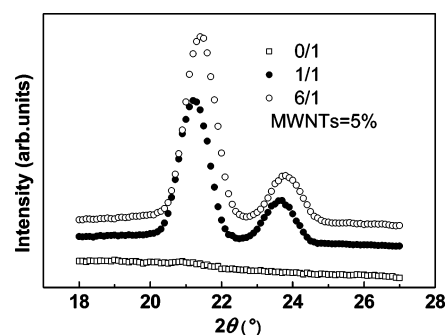


Figure 5. X-ray diffraction intensity for composites with 5% MWNTs.

conductivity of the composite slightly decreased as EMMA content decreased, and the drastic decrease was confirmed when the EMMA content became lower than 14% (the 6/1 composition). Namely, the conductivity was less than 10^{-7} S/cm for the 9/1 blend. Even so, EMMA itself is an insulator, but the admixture of the small amount of MWNTs provided drastic increase in the conductivity of the UHMWPE/EMMA composite. This behavior is probably thought to be due to the fact that polar side groups of EMMA hamper the crystallization of the EMMA chains on the MWNT surfaces, and then most of the MWNTs, which did not cover by the thick layer, are dispersed uniformly in the EMMA matrix. Accordingly, it may be expected that the coating on the MWNT surface by UHMWPE/EMMA is expanded from the surface area to inner part of the film with increasing UHMWPE content.

The Young's modulus of the composites as a function of EMMA content is also listed in Table 2. The value increases with decreasing the EMMA content, but the tendency is not significant. Table 2 indicates that the small amounts of the EMMA provided the drastic increase in electrical conductivity and very small decrease of Young's modulus.

Figure 5 shows X-ray diffraction intensity curves for the 0/1, 1/1, and 6/1 composites containing 5% MWNT content. A very weak broad peak for the EMMA-MWNT composite (0/1) appeared around 21° (twice the Bragg angle), as has been confirmed for the same profile of the neat EMMA whose crystallinity is ca. 9%.²⁶ The detailed analysis for X-ray diffraction of the neat EMMA²⁶ indicates that the component of the very weak-broad peak was attributed to the main contribution from amorphous phase and very small contribution from the (110) and (200) planes. This means that under the presence of the MWNTs the EMMA did not form crystallites with ordered lattice as detected by X-ray diffraction. The peak magnitude was more intense with increasing UHMWPE content, and the peak position shifted to higher angle. For the 6/1 composite, the diffraction peak tops for the (110) and (200) planes slightly shifted to lower sides than 21.6° and 24.0° , respectively, which indicates very small lattice fluctuation of the resultant crystallites in comparison with the perfectly ordered crystal lattice as observed usually for the neat UHMWPE²⁴ prepared by the gelation/crystallization method. These clear peak shifts to lower diffraction angle were also confirmed for the 1/1 composition. The shifts were reported to be attributed to the diffraction from crystallites with the disorder lattice expanded along the *a*-axis.²⁶ On the other hand, X-ray diffraction intensity profiles of the 1/1 and 6/1 composites with no MWNT

Table 2. Properties of Original Composites with 5% MWNTs as a Function of the Content of EMMA at the Room Temperature

UHMWPE/EMMA	0/1	1/1	2/1	6/1	9/1
conductivity (S/cm)	5.13×10^{-2}	2.05×10^{-3}	1.64×10^{-3}	9.12×10^{-4}	1.20×10^{-8}
Young's modulus (GPa)	3.92	4.23	4.62	4.91	5.04
energy gap (eV)	0.050	0.126	0.138	0.149	3.060

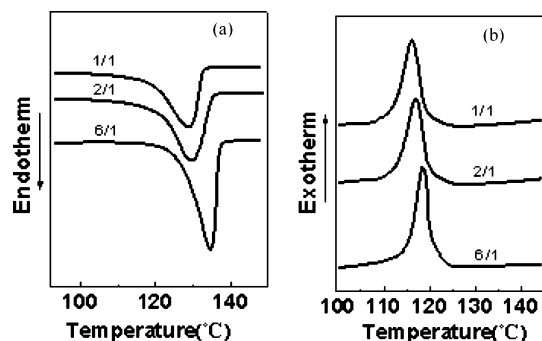


Figure 6. DSC curves of composites with 5% MWNTs: (a) heating process; (b) cooling process.

were equal to those with 5% MWNT, indicating that the crystallization was hardly affected by the admixture of the MWNTs. Accordingly, it was concluded that the admixture of the EMMA causes the lattice fluctuation of the polyethylene crystal unit and the crystallites within the blend become more unstable with increasing EMMA content. To obtain more conclusive evidence, DSC measurements were carried out.

Figure 6a,b shows the DSC curves under heating and cooling processes measured for the UHMWPE/EMMA–MWNT composites as a function of EMMA concentration, when MWNT content was fixed to be 5%. Under the heating process, a single endothermic peak was observed but the peak slightly shifted to higher temperature, and the magnitude was more intense with increasing UHMWPE content. But the endothermic peak of the compositions appeared below 134 °C. A series of experimental results indicate that the cocrystallization of the EMMA and the UHMWPE chains occurred under gelation/crystallization processes. If the cocrystallization did not occur within the composite, the large peak must appear at the melting temperature (137 °C) of only the UHMWPE crystallites observed for the undrawn UHMWPE film prepared by the same method. Judging from the decrease of melting point with increasing EMMA content, it may be expected that the cocrystallization occurred under the gelation/crystallization process.

As shown in Figure 6b, the exothermic peak shifted to lower temperature side with increasing EMMA content, indicating that the crystallization of the UHMWPE and the EMMA did not occur independently and the EMMA chains must be contained within the resultant cocrystallites. If this was not, the appearance of the exothermic peak must be the same temperature independent of EMMA content. Incidentally, the DSC curves under the heating and cooling processes showed the same profiles in the case of the composite without containing the MWNTs.

Parts a and b of Figure 7 show temperature dependence of electrical conductivity measured for the EMMA–MWNT and UHMWPE/EMMA–MWNT composites, respectively, in which the content of the MWNTs is 5%. Heating of the samples was carried out for three cycles termed as the first run, the second run, and the third run. As shown in Figure 7a, it is seen that the electrical conductivity of the EMMA–MWNT composite increased slightly at temperatures beyond 70 °C at the first heating run. However, the values at the second and third runs were almost equal to those at the first run. Incidentally, the temperature dependence of the EMMA film with 10% MWNT was also similar to this behavior, since the 5% was the saturation value for conductivity as shown in Figure 3. The temperature dependence of this MWNT sheet is shown together with those of the EMMA–MWNT composite in this figure. The electrical conductivity of the MWNTs was tested on a loosen MWNT sheet which was prepared by mixing them in methanol and then

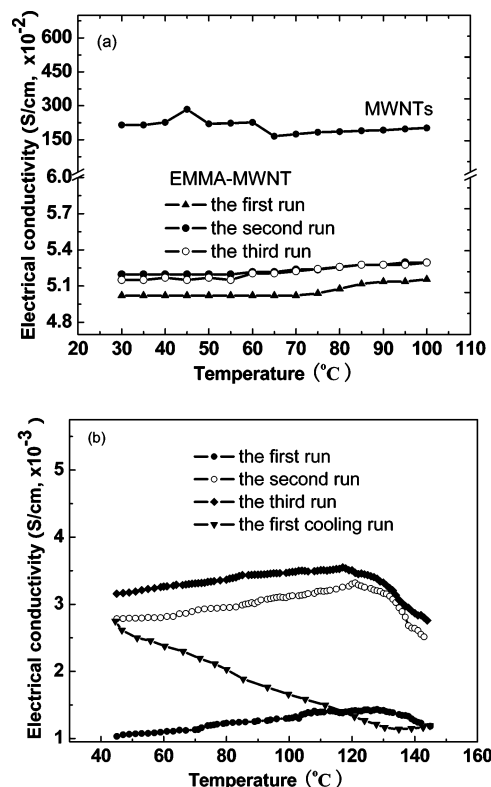


Figure 7. Temperature dependence of electrical conductivity measured for composites with 5% MWNTs: (a) EMMA; (b) UHMWPE/EMMA (6/1).

filtering. Here it should be noted that the measured conductivities of the sheet are much lower than the theoretical values reported somewhere.^{33,34} This is due to the defects of curved graphene sheets of MWNTs containing amorphous carbon regions, which provides the flexibility of MWNTs to form entanglements. If the MWNTs had no defects, the MWNTs must be straight tubes. Despite the entanglements of the MWNTs, the conductivity of the MWNT sheet was much higher than those of the EMMA–MWNT composites. This indicates the possibility that dispersed MWNTs were covered by very thin layer of the EMMA chains and active charge carrier between adjacent MWNTs hamper by the layer.

Figure 7b shows temperature dependence of the conductivity under the repeated heating cycles measured for the 6/1 composite containing 5% MWNTs. The conductivity increased with elevating temperature and tended to decrease with further heating beyond 120 °C. After the first heating run, the composite was cooled to room temperature. In the cooling process, the conductivity increased. The conductivity also increased with elevating temperature and decreased beyond 120 °C. Such behavior was also observed at the third heating run. The same tendency was also confirmed for the 2/1 and 1/1 composites containing 5% MWNTs. Under SEM observation, it was confirmed that the average thickness (diameter) of the UHMWPE/EMMA layer on the MWNT surface became thinner with increasing heating run, and the drastic decrease occurred after the first heating run. This indicated that the recrystallization of melted UHMWPE/EMMA chains under the cooling process did not occur on the MWNT surface mainly.

According to the previous paper for UHMWPE–MWNT containing 5% MWNT content,¹⁷ the conductivity increased from 10^{-12} to 10^{-5} S/cm by heating. For the first cycle, the conductivity increased with increasing temperature, when the

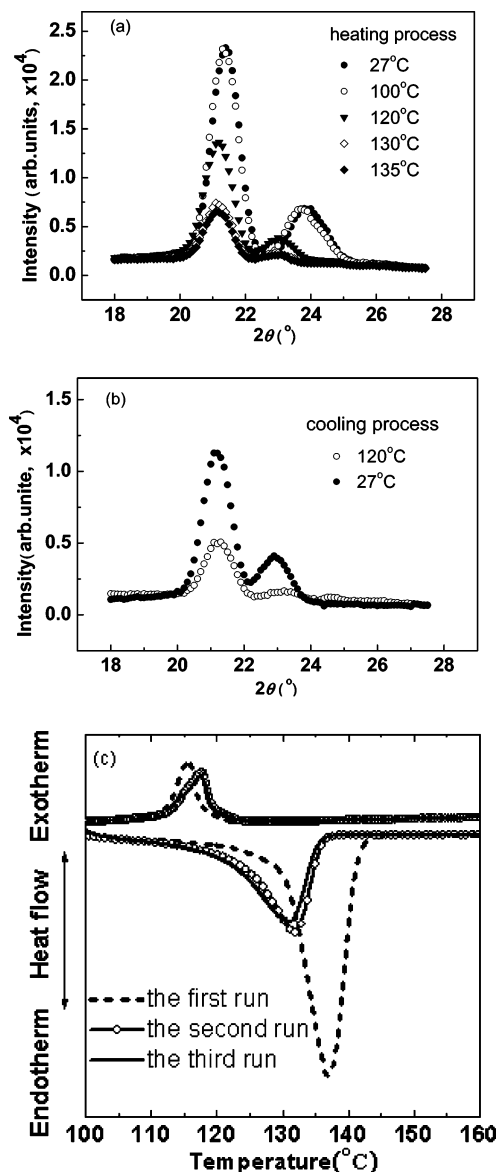


Figure 8. Temperature dependence of X-ray diffraction curves for the undrawn composites (6/1) with 5% MWNTs: (a) heating process, (b) cooling process, and (c) DSC analysis.

specimen was heated to the melting point of the UHMWPE. After cooling, the conductivity of the heat-treated composite was higher than that of the original composites. At the second heating, the conductivity maintained constant values up to 130 °C and tended to decrease slightly. In the second run, the temperature dependence of conductivity of the UHMWPE–MWNT composite was similar to the behavior of the UHMWPE/EMMA–MWNT, although the conductivity of the present UHMWPE/EMMA–MWNT composite was higher than that of the UHMWPE–MWNT composite in the given temperature range.

A question can be raised as to why the conductivity increased with elevating temperature up to 120 °C independent of the repeated heating run but it decreased beyond 120 °C. Such behavior has never been observed, and the inverse results could be reported for carbon black and UHMWPE.^{35,36} To obtain more detailed information, the temperature dependence of X-ray diffraction curves for the 6/1 composite containing 5% MWNT are shown in Figure 8a,b. Under the heating process, the diffraction peak intensities are almost constant up to 100 °C. In this temperature region, the electrical conductivity increases

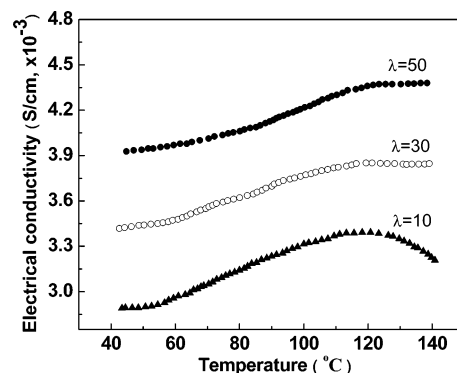


Figure 9. Temperature dependence of electrical conductivity measured for composites (6/1) with 5% MWNTs as the function of draw ratio.

with elevating temperature, as shown in Figure 7b. The X-ray diffraction peak decrease drastically at 120 °C, corresponding to the starting point of the decrease of the electrical conductivity (see Figure 7b) as well as the starting point of the melting of the crystallites (see Figure 8c). Further increase in temperature up to 135 °C caused further drastic decrease of the X-ray peak intensity, which is also related to the drastic decrease of the electrical conductivity. Under the cooling process from 140 to 27 °C, the measurements were done at 120 and 27 °C, which is shown in Figure 8b. The peak intensity increased with decreasing temperature, but an increase in the magnitude of the diffraction intensity peak associated with recrystallization by the cooling was much lower than the peak magnitude of the original film at the corresponding temperature. Namely, it is obvious that the sample after the first heating had morphology different from the original film prepared by gelation/crystallization, in which the morphology is obviously thought to be similar to that of the melted film. Such behavior of X-ray diffraction intensity satisfies the thermal properties estimated by DSC curves shown in Figure 8c. The DSC curves correspond to the above heating cycles. Namely, the endothermic peak at the first heating showed a large peak, indicating high crystallinity of the original film. But the exothermic peak under the first cooling showed a small peak, indicating that the crystallinity of the film prepared by cooling the original film is lower than that of the original film. Certainly the endothermic peaks under the second heating was much smaller than that of the original film, which supports the behavior of the X-ray diffraction curves under the first cooling. Of course, the recrystallization of the UHMWPE/EMMA did not occur on the MWNT surface, and the thickness of UHMWPE/EMMA layer became very thin and then the conductivity increased by the first heating and cooling cycle.

Figure 9 shows temperature dependence of the drawn UHMWPE/EMMA–MWNT (6/1) composites. Interestingly, the conductivity slightly increased with draw ratio, and it also increased with elevating temperature in the given range. This is quite different from the results of the UHMWPE–MWNT composites containing 5% and 15% MWNT contents reported already.¹⁷ According to the previous paper,¹⁷ the conductivity of the UHMWPE–MWNT composite with 5% MWNT decreased drastically and became an insulator when the sample was stretched beyond 20 times. Only for the composite with 15% MWNT content, the decrease of conductivity by the elongation up to 100 times could be prevented. The decrease in the conductivity was attributed to disappearance of electrical conductive paths due to the disruption of three-dimensional networks by the tension along the stretching direction. On the other hand, the conductivity of UHMWPE/EMMA composite

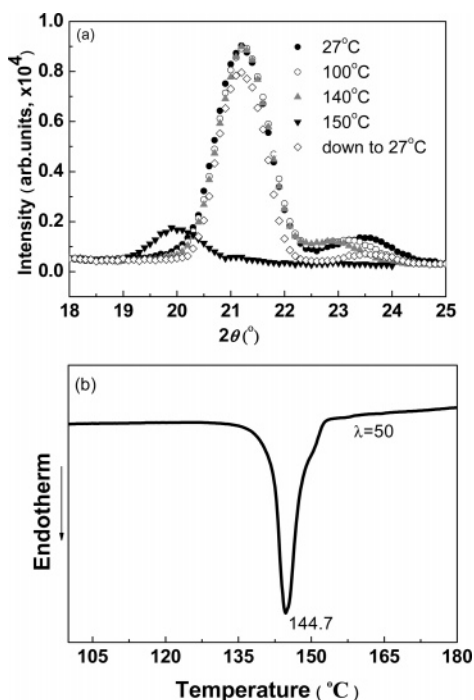


Figure 10. Temperature dependence of X-ray diffraction curves for composites (6/1) containing 5% MWNTs with $\lambda = 50$ under heating processes (a) and (b) DSC analysis.

with the 5% MWNT content was much higher than that of UHMWPE–MWNT with the same MWNT content. Interestingly, the conductivities of the composites with $\lambda = 30$ and 50 tended to level off beyond 120 $^\circ\text{C}$, which is different from the decrease of conductivity for the undrawn composite beyond 120 $^\circ\text{C}$, as shown in Figure 7b. To investigate this phenomenon, X-ray diffraction and DSC measurements were carried out for the composite with $\lambda = 50$.

Figure 10a shows temperature dependence of X-ray diffraction curves for the 6/1 composite containing 5% MWNT with $\lambda = 50$ under heating processes. The diffraction intensity maintained almost the same magnitude up to 140 $^\circ\text{C}$, but the peak disappeared suddenly at 150 $^\circ\text{C}$ and the amorphous halo appeared around 19.8 $^\circ$, indicating the melting of crystallites. To persuade the above analysis, the corresponding DSC curve is shown in Figure 10b. It can be seen that the partial melting started at 135.0 $^\circ\text{C}$ and the endothermic peak top was 144.7 $^\circ\text{C}$. This behavior supports the drastic decrease in the X-ray diffraction peak magnitude in the temperature range 140–150 $^\circ\text{C}$ in Figure 10a.

Here it should be noted that the diffraction intensity measured again at 27 $^\circ\text{C}$ after the cooling recovered to the peak profile close to the intensity magnitude of the original composite. This means that when extended crystallites changed to the extended amorphous chains by melting, the perfect recovery from the extended amorphous chains to the extended crystallites occurred by cooling. Namely, the amorphous chains in the melt state were obliged to retain the extended chain arrangement, since the specimen was fixed at a constant length under the heating process to ensure X-ray diffraction geometry. The crystallinities were almost constant in the temperature range from 27 to 140 $^\circ\text{C}$, and the corresponding electrical conductivity assured a slight increase beyond 120 $^\circ\text{C}$ (see Figure 9). In contrast, as discussed in Figures 7b, the drastic decrease of the conductivity beyond 120 $^\circ\text{C}$ was confirmed for the undrawn composite, and the corresponding crystallinity also decreased. Accordingly, it is evident that no decrease in crystallinity beyond 120 $^\circ\text{C}$ provided

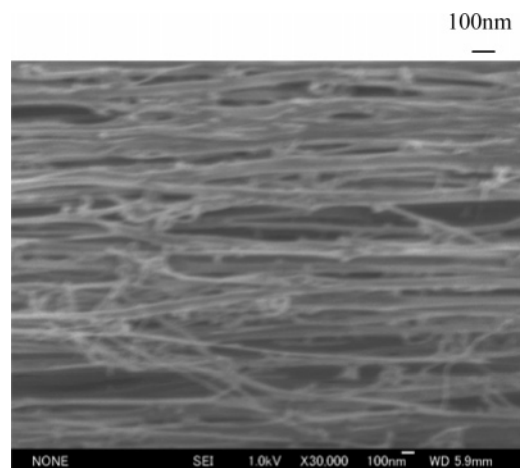


Figure 11. SEM image on the film surface of composite (6/1) containing 5% MWNT with $\lambda = 50$.

a slight increase in the electrical conductivity for the drawn composite with $\lambda = 50$. A series of experiments indicate that the increase in conductivity with increasing crystallinity is attributed to the electronic transition, and then the electrons transfer easily within the crystallites with short chain distance rather than the transfer within the amorphous region. Then the conductivities of the drawn films with $\lambda = 30$ and 50 are considered to be higher than that of undrawn film. This is quite different from the results for UHMWPE–MWNT system,¹⁷ as discussed before.

As shown in Figure 10b, the DSC peak of the UHMWPE/EMMA composite containing 5% MWNT at $\lambda = 50$ appeared at temperature (144.7 $^\circ\text{C}$) lower than the peak (145.8 $^\circ\text{C}$) of the neat UHMWPE film with the same draw ratio.¹⁷ These results indicate the cocrystallization of the EMMA and the UHMWPE chains under elongation and cooling processes. If cocrystallization of the EMMA and the UHMWPE chains within the blend film did not occur under elongation, the large peak must appear at the same temperature (145.8 $^\circ\text{C}$) as observed for the neat UHMWPE film, reflecting only the melting of UHMWPE crystallites. Judging from the melting point of the EMMA being much lower than that of the UHMWPE, the mechanism of cocrystallization under elongation is thought to be due to an epitaxial nucleation surface for oriented ethylene sequences of the oriented EMMA chains under cooling process to room temperature after elongation. Namely, the ethylene sequences of the melted EMMA were oriented by the shear stress, leading to the orientation of the UHMWPE chains with respect to the stretching direction, and they promoted the growth of crystallites on the surface of extended crystal chains of the UHMWPE under the cooling process. This means that the most of the extended amorphous EMMA chains cocrystallized with the extended UHMWPE chains on the boundary. The cocrystallization provided the small lattice fluctuation leading to the slightly lower melting point of the cocrystallites in comparison with the melting point of the neat UHMWPE crystallites. Incidentally, it was confirmed that the magnitude of endothermic peak of the composite with $\lambda = 50$ is highest among the three specimens ($\lambda = 10, 30$, and 50) and the corresponding melting point, 144.7 $^\circ\text{C}$, is the highest. This means that the crystallinity of the composite with $\lambda = 50$ was highest among the three composites.

Figure 11 shows SEM image on the surface of the 6/1 composite containing 5% MWNT with $\lambda = 50$. The observation reveals that most of the UHMWPE fibrils were oriented with respect to the stretching direction, but some of them formed

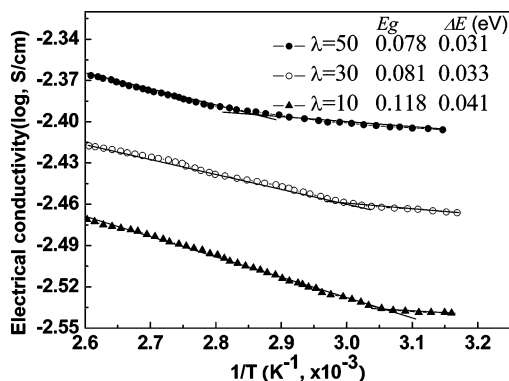


Figure 12. Conductive modes in the given temperature range for the drawn composites with $\lambda = 10, 30$, and 50 .

the continuous networks. Of course, it was confirmed that the corresponding WAXD patterns showed very sharp spots from the (110) and (200) planes, indicating very highly orientation of crystallites with respect to the stretching direction. In Figure 11, the average width (diameter) of fibrils was in the range 50–100 nm, and any MWNTs could not be observed. This indicates that each MWNT or each bundle as aggregation of some MWNTs was covered by the thin UHMWPE–EMMA layers, and the neighbor MWNT or the neighbor bundle covered by the layer did not contact each other directly. Together with other two SEM images of the specimens with $\lambda = 10$ and 20 (not shown in this paper), it is confirmed that average width (diameter) of the fibrils became thinner as the draw ratio increased. Accordingly, it may be expected that charge carrier between nearest MWNTs by hopping became easier with increasing draw ratio, and then the conductivity of the film with $\lambda = 50$ became slightly higher than those with $\lambda = 10$ and 30 . Of course, the electron transfer may be active at elevated temperature because of the increase in conductivity shown in Figure 9. However, when the crystallinity of the layer became lower with elevating temperature beyond 140°C as shown in Figure 10, the electric conductivity of the film became lower. This is probably due to the fact that the electron transfer from a MWNT to the adjoining MWNT due to electron transition mechanism became less active with decreasing crystal regions with overlapped electron clouds.

To elucidate more detailed conductive mechanism of the undrawn and drawn composites, the temperature dependence of the electrical conductivity was measured from 25 to 140°C (298 to 412 K). Figure 12 shows electrical conductivity against the derivative of absolute temperature plotted from the results (see Figure 9) for the drawn composites with $\lambda = 10, 30$, and 50 , which reveals the two different conductive modes in the given temperature range. Hence, the conductivity σ may be described as follows:^{37,38}

$$\sigma = \sigma_0 \exp\left(-\frac{E_g}{2kT}\right) + \sigma_e \exp\left(-\frac{\Delta E}{2kT}\right) \quad (1)$$

The former part corresponds to the conductive mode at high temperature and the latter to that of the low temperature range. In the viewpoint of a semiconductive band model, it is well-known that there are two kinds of electric carrier generation in a specimen. One is intrinsic carrier generation, in which the electrons in the valence band move directly to the conducting band by hopping over the energy gap of E_g . The other is the extrinsic carrier generation, in which electrons, combined in localized levels, are excited to the conducting band and free carriers are mostly generated. As shown in Figure 12, E_g may

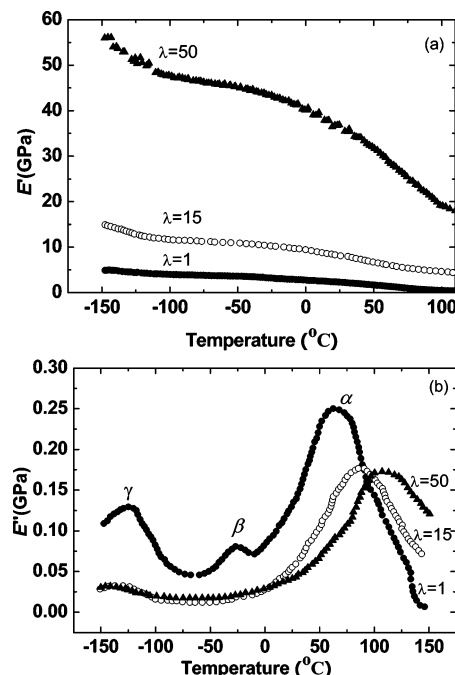


Figure 13. Temperature dependence of the storage modulus E' (a) and loss modulus E'' (b) measured for composites (6/1) with 5% MWNTs.

be obtained from the slope of the plots against the reciprocal of absolute temperature ($\log \sigma - 1/T$). In the lower temperature range, the excited electrons from impurity (donor) levels to the conducting band and electrons from the valence band to impurity (acceptor) levels increase in comparison with the electrons which are host-excited from the valence band to the conducting band. The energy difference between the impurity level and the valence band (or the conducting band) is confirmed as ΔE .^{39,40} The values of E_g and ΔE are listed in Figure 12. It is obvious that ΔE is much smaller than E_g . The energy gap E_g became smaller with increasing draw ratio. This is due to the fact that the average thickness (diameter) of the UHMWPE/EMMA layer became thinner with increasing draw ratio. By the same method, the value of E_g for undrawn films calculated on the basis of the results in Figure 7b is listed together in Table 2. The value of E_g becomes lower with increasing EMMA content. These results are in good agreement with the experimental results that electric conductivity increased with increasing EMMA content and draw ratio.

Figure 13 shows the temperature dependence of the storage modulus E' and loss modulus E'' measured for the 6/1 composites with 5% MWNT. The storage modulus increased with increasing draw ratio. Even though E' for the specimen with $\lambda = 50$ was lower than E' for the neat UHMWPE reported elsewhere,¹⁷ it is of interest that E' is beyond 37 GPa close to the crystal lattice modulus of polypropylene along the crystal chain direction,⁴¹ indicating successful results for preparing polymeric materials with high modulus and high conductivity.

The temperature dependence of E'' is sensitive to the draw ratio. Three dispersion peaks termed as α , β , and γ relaxations from higher temperature side are observed for the undrawn film. The α dispersion is essentially associated with crystal relaxation from cocrystallites of the UHMWPE and EMMA, and the peak becomes larger with increasing draw ratio and shifts to higher temperature range, indicating an increase in crystallinity. The β relaxation appeared at around -25°C .

In accordance with the previous work for the relaxation mode of UHMWPE–EMMA blends in terms of mechanical and

positron annihilation methods,⁴² it is concluded that the β relaxation is not assigned as a glassy transition but is associated with a large motion of amorphous chains. The β relaxation peak magnitude disappeared by elongation up to 15 times. The disappearance is thought to be due to an effect of the epitaxial nucleation surface of the ethylene sequences of the EMMA chains. Namely the EMMA chains crystallized on the surface of the UHMWPE crystallites behave as crystalline mode different from a large motion as amorphous chains, when EMMA content is much less than UHMWPE content. However, when the blend film with 50% EMMA content (1/1 composition) was stretched up to 100 times, the β relaxation peak appeared, indicating that most of the oriented EMMA chains within the 1/1 blend exist as an amorphous state with highly ordered arrangement and/or unstable state with large fluctuation of the lattice distance.²⁴ In the present case, the ethylene sequences of the EMMA chains crystallize mainly together with UHMWPE chains on the MWNT surfaces, as shown in Figure 11. Hence the γ relaxation, associated with the local chain in the amorphous phase, was observed for the undrawn composite at around $-130\text{ }^{\circ}\text{C}$, but the peak disappeared at $\lambda = 15$. This is in good agreement with the behavior of the β relaxation.

Finally, we must emphasize that a series of experimental results must be taken into consideration on the basis of recent concepts^{43–46} concerning conductive polymers in terms of charge carrier. In doing so, more detailed information on polymer and MWNT composite materials must be needed in terms of the change in electric current density against voltage.

4. Conclusion

The UHMWPE/EMMA composites containing desired MWNT contents were prepared by the gelation/crystallization method. EMMA is itself an insulator like UHMWPE, but the drastic increase in electrical conductivity could be realized by admixing 5% MWNT content. Such drastic increase in conductivity could not be confirmed even for the UHMWPE–MWNT whose MWNT content was 15%. This suggested that the polar side groups of the EMMA chains did not form thick layers on MWNT surface which disturb active electron transfer between adjacent MWNTs. The admixture of the EMMA into the UHMWPE also provided drastic increase in conductivity, when MWNT content was 5%. The conductivity of the UHMWPE/EMMA composite containing 5% MWNT increased with increasing draw ratio up to 50 times, since the average thickness (diameter) of the UHMWPE/EMMA layers become thinner with increasing draw ratio. The conductivity increased with elevating temperature, but it decreased when temperature was close to the melting point of the UHMWPE/EMMA cocrystallites because of the decrease of crystal regions. This indicated that the band gap became longer by an increase in fluctuation of ordered chains. Accordingly, it turned out that the electron transfer from a MWNT to the adjoining MWNT is due to electronic transition mechanism, and the electron transfer becomes easier with increasing crystal regions with overlapped electron clouds. On stretching up to 50 times, Young's modulus of the 6/1 blend film containing 5% MWNT reached 37 GPa close to ultimate goal (41 GPa) of crystal lattice modulus along the crystal chain direction of polypropylene. Therefore, it may be concluded that the present method is one of the successful techniques to prepare high electrical conductivity with high modulus.

References and Notes

- Pötschke, P.; Bhattacharyya, A. R.; Janke, A. *Polymer* **2003**, *44*, 8061–8069.
- Safadi, B.; Andrews, R.; Grulke, E. A. *J. Appl. Polym. Sci.* **2002**, *84*, 2660–2669.
- Sandler, J.; Shaffer, M. S. P.; Prasse, T.; Bauhofer, W.; Schulte, K.; Windle, A. H. *Polymer* **1999**, *40*, 5967–5971.
- Ajayan, P. M.; Schadler, L. S.; Giannaris, C.; Rubio, A. *Adv. Mater.* **2000**, *12*, 750–753.
- Haggenmueller, G. H. R.; Rinzler, A. G.; Fischer, J. E.; Winey, K. I. *Chem. Phys. Lett.* **2000**, *330*, 219–225.
- Thostensson, E. T.; Renb, Z.; Choua, T. W. *Compos. Sci. Technol.* **2001**, *61*, 1899–912.
- Paiva, M. C.; Zhou, B.; Fernando, K. A. S.; Lin, Y.; Kennedy, J. M.; Sun, Y. P. *Carbon* **2004**, *42*, 2849–2854.
- Kimura, T.; Ago, H.; Tobita, M.; Ohshima, S.; Kyotani, M.; Yumura, M. *Adv. Mater.* **2002**, *14*, 1380–1383.
- Haggenmueller, R.; Gommans, H. H.; Rinzler, A.; Fischer, J. E.; Winey, K. I. *Chem. Phys. Lett.* **2000**, *330*, 219–225.
- Thongruang, W.; Balik, C. M.; Spontak, R. J. *J. Polym. Sci., Part B* **2002**, *40*, 1013–1023.
- Shaffer, M. S. P.; Windle, A. H. *Adv. Mater.* **1999**, *11*, 937–941.
- He, J. X.; Du, J. H.; Ying, Z.; Cheng, H. M. *Appl. Phys. Lett.* **2005**, *86*, (062112)1–3.
- Xi, Y.; Ishikawa, H.; Bin, Y. Z.; Matsuo, M. *Carbon* **2004**, *42*, 1699–1706.
- Chan, C. M.; Cheng, C. L.; Yuen, M. M. F. *Polym. Eng. Sci.* **1997**, *37*, 1127–1136.
- Lee, G. J.; Suh, K. D.; Im, S. S. *Polym. Eng. Sci.* **2000**, *40*, 247–255.
- Chan, C. M. *Polym. Eng. Sci.* **1996**, *36*, 495–500.
- Bin, Y. Z.; Kitanaka, M.; Zhu, D.; Matsuo, M. *Macromolecules* **2003**, *36*, 6213–6219.
- Manchado, M. A. L.; Valentini, L.; Biaiotti, J.; Kenny, J. M. *Carbon* **2005**, *43*, 1499–1505.
- Ruan, S. L.; Gao, P.; Yang, X. G.; Yu, T. X. *Polymer* **2003**, *44*, 5643–5654.
- Thostenson, E. T.; Chou, T. W. *J. Phys. D: Appl. Phys.* **2002**, *35*, L77–L80.
- Shaffer, M. S. P.; Windle, A. H. *Adv. Mater.* **1999**, *11*, 937–941.
- Jia, W. T.; Chen, X. F. *J. Appl. Polym. Sci.* **1997**, *66*, 1885–1890.
- Peng, G. W.; Qiu, F.; Ginzburg, V. V.; Jasnow, D.; Balazs, A. *Science* **2000**, *288*, 1802–1804.
- Ma, L.; Azuma, M.; He, C. Q.; Suzuki, T.; Bin, Y. Z.; Matsuo, M. *Macromolecules* **2004**, *37*, 7673–7682.
- Zhang, Q.; Lippitz, D. R.; Rastogi, S. *Macromolecules* **2006**, *39*, 658–666.
- Ma, L.; Bin, Y. Z.; Sakai, Y.; Chen, Q.; Kurosu, H.; Matsuo, M. *Macromolecules* **2001**, *34*, 4802–4814.
- Ma, L.; He, C.; Suzuk, T.; Azuma, M.; Bin, Y.; Kurosu, H.; Matsuo, M. *Macromolecules* **2003**, *36*, 8056–8065.
- Nemanish, R. J.; Solin, S. A. *Phys. Rev. B* **1979**, *20*, 392–398.
- An, C. P.; Vardeny, Z. V.; Iqbal, Z.; Spinks, G.; Baughman, R. H.; Zakhidov, A. *Synth. Met.* **2001**, *116*, 411–413.
- Matsuo, M.; Sawatari, C. *Macromolecules* **1986**, *19*, 2028–2035.
- Matsuo, M.; Sawatari, C. *Macromolecules* **1988**, *21*, 1653–1658.
- Matsuo, M.; Sawatari, C.; Ohhata, T. *Macromolecules* **1988**, *21*, 1317–1324.
- Yang, D. J.; Wang, S. G.; Zhang, Q.; Sellin, P. J.; Chen, G. *Phys. Lett. A* **2004**, *329*, 207–213.
- Hoenlein, W.; Kreupl, F.; Duesberg, G. S.; Graham, A. P.; Liebau, M.; Seidel, R.; Unger, E. *Mater. Sci. Eng.* **2003**, *C23*, 663–669.
- Xu, C.; Agari, Y.; Matsuo, M. *Polym. J.* **1998**, *30*, 372–380.
- Bin, Y.; Xu, C.; Zhu, D. Matsuo, M. *Carbon* **2002**, *40*, 195–199.
- Figueiredo, J. L.; Bernardo, C. A.; Baker, P. T. K.; Huttering, K. J. *Carbon Fibers Filaments and Composites*; Klumer Academic Publishers: Dordrecht, 1989.
- Sasahe, H. *Conductive Polymic Materials*; CMC Publishers: 2000.
- Ibrahim, A. S.; Attla, G.; Abo-ellil, M. S.; Abdel-kader, F. H. *Appl. Polym. Sci.* **1997**, *63*, 343–348.
- Saad, A. L. G.; Aziz, H. A.; Dimitry, O. I. H. *J. Appl. Polym. Sci.* **2004**, *91*, 1590–1598.
- Sawatari, C.; Matsuo, M. *Macromolecules* **1986**, *19*, 2653–2656.
- Matsuo, M.; Ma, L.; Azuma, M.; He, C.; Suzuki, T. *Macromolecules* **2002**, *35*, 3059–3065.
- Novikov, S. V.; Dunlap, D. H.; Kenkre, V. M.; Parris, P. E.; Vannikov, A. V. *Phys. Rev. Lett.* **1998**, *81*, 4472–4478.
- Novikov, S. V. *J. Polym. Sci., Part B: Polym. Phys.* **2003**, *41*, 2584–2594.
- Tanase, C.; Meijer, E. J.; Blom, P. W. M.; de Leeuw, D. M. *Phys. Rev. Lett.* **2003**, *91*, 216601–9.
- Pasveer, W. F.; Cottaar, J.; Tanase, C.; Coehoorn, R.; Bobbert, P. A.; Blom, P. W. M. *Phys. Rev. Lett.* **2005**, *94*, 206601–4.